C. R. Mecanique 344 (2016) 661–671

Contents lists available at ScienceDirect

Comptes Rendus Mecanique

www.sciencedirect.com

Bifurcation analysis of a flexible balanced cracked rotor–bearing system

Nizar Ferjaoui *, Sami Naimi, Mnaour Chouchane

Laboratory of Mechanical Engineering, National Engineering School of Monastir, University of Monastir, avenue Ibn Eljazzar, 5019 Monastir, Tunisia

ARTICLE INFO

Article history:
Received 9 March 2016
Accepted 2 June 2016
Available online 22 July 2016

Keywords:
Cracked rotor
Nonlinear dynamic analysis
Bifurcation diagram
Hydrodynamic bearings

ABSTRACT

The dynamic analysis of cracked rotors is of considerable current interest. In the present paper, the effect of the presence of a transverse crack in a rotor supported by two hydrodynamic journal bearings is investigated. A nonlinear model of a flexible cracked rotor–bearing system is proposed. The model of the hydrodynamic forces is derived based on the assumption of a short bearing approximation and a half-Sommerfeld boundary condition. The system of nonlinear differential equations is integrated numerically using the Runge–Kutta method. The effect of the crack depth on the motion of the journal center in the vicinity of the stability limit is investigated. Bifurcation diagrams and Poincaré maps are used to determine the effect of the crack on the stability limit and on the journal motion.

1. Introduction

A crack defect in a rotor is generally considered a sever fault. The dynamic analysis of cracked rotors is a problem of great interest due to its practical importance; consequently, it has received considerable attention in the last decades. The presence of a crack affects the dynamic response of a rotor because of the reduction in the rotor's stiffness and thus in the natural frequencies of the original uncracked rotor [1]. Different approaches have been proposed for dynamic analysis of a cracked rotor based on two established models. The first one is the model of opening and closing crack, or switching model. In this model, the stiffness of the rotor varies between the stiffness corresponding to the closed crack and the stiffness corresponding to the open crack. In the second model, known as the breathing crack model, a partial opening/closing of the crack is modeled using a periodic function that governs the change in stiffness. Several studies have considered the effect of a crack on the stability of the rotor using several methods to model the presence of a crack. Papadopoulos and Dimarogonas [2] used an analytical approach to compute the local flexibility of a cracked shaft using the strain energy and the stress intensity. This approach has been validated by experimental results. Sekhar and Prabhu [3] computed the natural frequencies and mode shapes of a cracked rotor using a Finite Element Model. The detection of a crack in the shaft is based on the variation of natural frequencies. Mayes and Davies [4] studied the presence of a crack using the switching crack model. The opening and closing of the crack are modeled by a truncated Fourier series. Mancilla and Sinou [5] showed, using a numerical simulation, that the evolution of the orbit of the journal center on the one-half and one-third first

* Corresponding author.
E-mail address: nizar.ferjaoui@isetkh.rnu.tn (N. Ferjaoui).

http://dx.doi.org/10.1016/j.crme.2016.06.001
1631-0721/

Nomenclature

m	rotor mass per bearing
g	gravity constant
$\{Z\} = \{x\ y\}^{\mathrm{T}}$	vector of the disk displacements in inertial coordinates
a	depth of the crack
d	diameter of the shaft
$r = a/d$	dimensionless crack depth ratio
l	length of the shaft
C	bearing radial clearance
$e = \overline{O_b O_j}$	bearing eccentricity
$\varepsilon = e/C$	relative eccentricity
ω	angular velocity
$\varpi = \omega\sqrt{C/g}$	dimensionless journal angular velocity
$\tau = \omega t$	dimensionless time
ϕ	attitude angle
β	torsional angle
ξ, η	rotating coordinates, ξ along crack orientation, η perpendicular to the crack orientation
O_{b}	bearing center
O_{j}	dynamic position of the journal center
f_ε, f_ϕ	radial and tangential components of the hydrodynamic forces
K	half shaft stiffness
$\Delta K_\xi, \Delta K_\eta$	stiffness changes due to crack, in ξ and η directions
Δk_ξ	dimensionless stiffness change along ξ direction ($\Delta k_\xi = \Delta K_\xi / K$)
Δk_η	dimensionless stiffness change along η direction ($\Delta k_\eta = \Delta K_\eta / K$)
$\bar{K} = K(C/mg)$	dimensionless stiffness of the uncracked shaft
$\Gamma = \mu R L^3/(2mC^{2.5}g^{0.5})$	bearing parameter
μ	constant lubricant viscosity
$g(\omega t)$	crack function that defines the angular position of the crack
k_{ij} $(i = x, j = y)$	stiffness matrix coefficients
$[K_{\mathrm{R}}]$	stiffness matrix of the rotor system in rotating coordinate system
$[K_{\mathrm{I}}]$	stiffness matrix of the rotor system in inertial coordinate system
$[M]$	rotor mass matrix

frequency can be used to detect rotor cracks. Sinou and Lees [6] evaluated the dynamic response of a rotor with a breathing crack by using the time-frequency domain approach. The increase in the harmonic components of the dynamic system response and the evolution of the size of the orbit are the principal indicators of the presence of a crack in a rotating shaft. Later, they have used the Harmonic Balance Method to study the influence of a crack on the dynamic response of a rotor. The evolution of the trajectory center of the rotor near half of the first critical speed is an indication of the existence of a crack [7]. Xue and Cao [8] used the Runge–Kutta method to solve a system of differential equations of a cracked rotor. Bifurcation diagrams, Poincaré sections and rotor trajectory diagrams are used to study the effect of rotating speed, and crack depth on the dynamic response of the rotor. The onset of a period doubling orbit is considered an indicator of the presence of a crack in the shaft. The domain of instability increases considerably when the crack deepens.

A nonlinear model of a cracked rotor–bearing system is used by Luo and Zhang [9]. Harmonic frequency method is used to study the presence of the crack. The analysis proves that the increase of the depth of a crack reduces the stability limit of the system. Chaofeng and Hexing [10] used the Finite Element Method to study the stability of a nonlinear cracked rotor–bearing system. To study the effect of the depth of the crack on the stability of the rotor as a function of the rotor speed, they used bifurcation diagrams, Poincaré sections, and trajectories of the shaft center. They also showed that the crack fault reduces the stability speed of the rotor as the crack becomes deeper. The simulation results have been validated experimentally. In this study, they showed that the stability speed limit decreases as the crack becomes deeper. Gasch [11] used Floquet theory to study the effect of a crack in the vibrations signal. He showed that a deeper crack in the shaft changes the natural frequencies, and that the crack detection, in practice, is difficult for cracks depth less than 25%.

In this paper, a four-degree-of-freedom dynamic model of a perfectly balanced flexible cracked rotor supported by hydrodynamic journal bearings is derived. The fluid film force components corresponding to the half Sommerfeld conditions for a short hydrodynamic bearing are used ($L/D \leq 0.25$). Bifurcation diagrams and trajectories of the journal center have been used to predict the effect of the crack depth on the limits of the stability and its motion in the vicinity of the stability limit. The validity of this research is proved by the detection of a crack in the journal using bifurcation diagrams, Poincaré sections, trajectories of the journal center and power spectra.

2. A nonlinear model of a balanced flexible cracked rotor–bearing system

Fig. 1 shows a symmetrical balanced flexible cracked rotor that has a mass $2m$ supported by two identical hydrodynamic short bearings O_{b} is the bearing center, O_{j} is the dynamic position of the journal center and f_ε, f_ϕ are respectively the radial and tangential components of the hydrodynamic forces applied on each journal bearing.

To analyze the dynamic response of a flexible balanced cracked rotor, the following assumptions are used:

(a) the deflection of the shaft is sufficiently small to permit the use of classical linear beam theory;
(b) due to the short bearing assumption and lubricant force description, the length to diameter, L/D, has to be less or equal to 0.25;

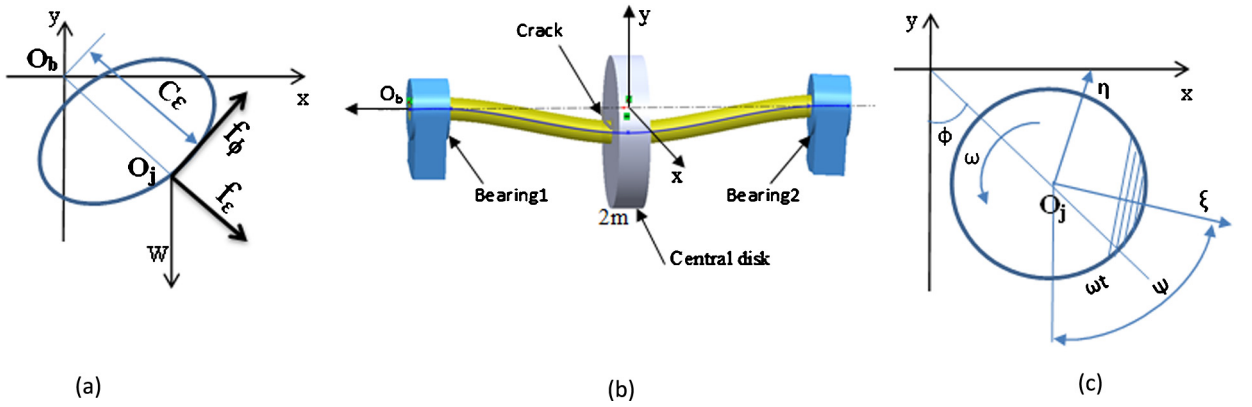

Fig. 1. (a) Hydrodynamic forces applied on the journal. (b) A general view of the rotor. (c) Coordinate system associated with the crack.

(c) motion at the bearings is supposed to be perfectly symmetrical; moreover, due to its nonlinear character, this includes having exactly the same initial conditions, I.C.s.;
(d) the rotor mass is lumped at the mid-point with a massless shaft, a central load of 2 mg and an effective shaft stiffness $2K$ (K is the effective stiffness of the half-rotor);
(e) the gyroscopic effects of the journal and of the central disk are negligible.

The equations of motion for the journal center in Cartesian coordinates are derived using the equilibrium equation of forces on the journal as follows [11,12]:

$$\begin{bmatrix} \sin\phi & \cos\phi \\ -\cos\phi & \sin\phi \end{bmatrix} \begin{Bmatrix} f_\varepsilon \\ f_\phi \end{Bmatrix} + \begin{bmatrix} K & 0 \\ 0 & K \end{bmatrix} \begin{Bmatrix} x - C\varepsilon\sin\phi \\ y + C\varepsilon\cos\phi \end{Bmatrix} = \begin{Bmatrix} 0 \\ 0 \end{Bmatrix} \tag{1}$$

According to the short bearing theory and the half Sommerfeld condition, the dimensionless radial and tangential components of the fluid film forces are [13]:

$$\begin{aligned} \bar{f}_\varepsilon &= \frac{f_\varepsilon}{mC\omega^2} = -\frac{\Gamma}{\varpi}\left[\frac{2\varepsilon^2(1-2\dot{\phi})}{(1-\varepsilon^2)^2} + \pi\frac{(1+2\varepsilon^2)\dot{\varepsilon}}{(1-\varepsilon^2)^{2.5}}\right] \\ \bar{f}_\phi &= \frac{f_\phi}{mC\omega^2} = \frac{\Gamma}{\varpi}\left[\pi\frac{(1-2\dot{\phi})\varepsilon}{2(1-\varepsilon^2)^{1.5}} + \frac{4\varepsilon\dot{\varepsilon}}{(1-\varepsilon^2)^2}\right] \end{aligned} \tag{2}$$

where $\Gamma = \mu RL^3/(2mC^{2.5}g^{0.5})$ is the bearing parameter and $\varpi = \omega\sqrt{C/g}$ is the dimensionless rotor speed. A2 × 2 inverse matrix is used in the bearing forces, Eq. (2), provides Eq. (3).

$$\begin{Bmatrix} \dot{\varepsilon} \\ \dot{\phi} \end{Bmatrix} = \begin{Bmatrix} 0 \\ -0.5 \end{Bmatrix} + \frac{1}{\varpi\Gamma(\pi^2 + 2(\pi^2-8)\varepsilon^2)} \begin{bmatrix} \pi(1-\varepsilon^2)^{2.5} & -4\varepsilon(1-\varepsilon^2)^2 \\ 4(1-\varepsilon^2)^2 & -\frac{2\pi(1-\varepsilon^2)^{1.5}(1+2\varepsilon^2)}{\varepsilon} \end{bmatrix} \begin{Bmatrix} \bar{f}_\varepsilon \\ \bar{f}_\phi \end{Bmatrix} \tag{3}$$

The stiffness matrix for the cracked shaft in rotating coordinates (ξ, η), defined in Fig. 1c, can be written as [1]:

$$[K_R] = \begin{bmatrix} k_\xi & 0 \\ 0 & k_\eta \end{bmatrix} = \begin{bmatrix} K & 0 \\ 0 & K \end{bmatrix} - g(\omega t)\begin{bmatrix} \Delta k_\xi & 0 \\ 0 & \Delta k_\eta \end{bmatrix} \tag{4}$$

where the first matrix in the right-hand side of Eq. (4) represents the stiffness of the uncracked shaft, and the second matrix represents the change in stiffness Δk_ξ and Δk_η in the ξ and η directions. The crack function $g(\omega t)$ describes the angular position of the crack defined as follows [11]:

$$g(\omega t) = \frac{1+\cos(\omega t)}{2} \tag{5}$$

The stiffness matrix for the rotor with a cracked shaft in inertial coordinates is given by [14]:

$$[K_I] = \begin{bmatrix} k_{xx} & k_{xy} \\ k_{yx} & k_{yy} \end{bmatrix} = \begin{bmatrix} K & 0 \\ 0 & K \end{bmatrix} - g(\omega t)\frac{K}{2}\begin{bmatrix} \Delta k_1 + \Delta k_2\cos(2\omega t) & \Delta k_2\sin(2\omega t) \\ \Delta k_2\sin(2\omega t) & \Delta k_1 - \Delta k_2\cos(2\omega t) \end{bmatrix} \tag{6}$$

where $\Delta k_1 = \Delta k_\xi + \Delta k_\eta$; $\Delta k_2 = \Delta k_\xi - \Delta k_\eta$.

The nonlinear coupled equations of motion of the balanced flexible cracked rotor can be written in inertial coordinate frame as:

$$[M]\{\ddot{Z}\} + [K_I]\{Z\} = \begin{Bmatrix} 0 \\ -mg \end{Bmatrix} \tag{7}$$

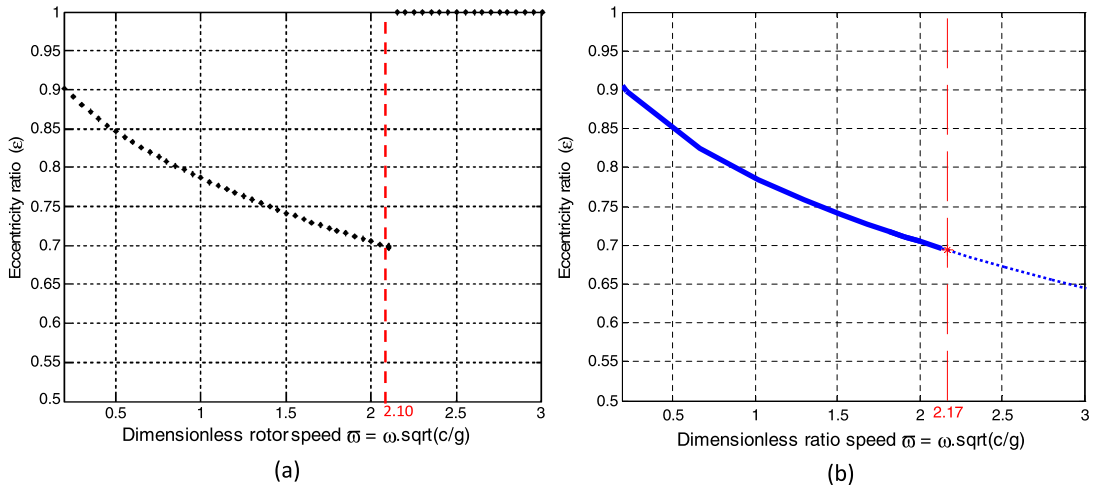

Fig. 2. Bifurcation diagrams of a balanced flexible rotor for $\Gamma = 0.1$ and $\bar{K} = 1$: (a) numerical integration, (b) numerical continuation.

where $[M] = \begin{bmatrix} m & 0 \\ 0 & m \end{bmatrix}$ is the rotor mass matrix and $\{Z\} = \{x - C\varepsilon\sin(\phi)\, y + C\varepsilon\cos(\phi)\}^{\mathrm{T}}$ is the vector of the disk displacements relative to the journal motion. The parameters ε, ϕ, x and y are all functions of time t.

Using equations (6) and (7), the dimensionless form of the equations of motion is obtained.

$$\begin{Bmatrix} \bar{\ddot{x}} \\ \bar{\ddot{y}} \end{Bmatrix} = -\frac{\bar{K}}{\varpi^2}\left(\begin{bmatrix} 1 & 0 \\ 0 & 1 \end{bmatrix} - \frac{g(\tau)}{2}\begin{bmatrix} \Delta k_1 + \Delta k_2\cos(2\tau) & \Delta k_2\sin(2\tau) \\ \Delta k_2\sin(2\tau) & \Delta k_1 - \Delta k_2\cos(\tau) \end{bmatrix}\right)\begin{Bmatrix} \bar{x} - \varepsilon\sin(\phi) \\ \bar{y} + \varepsilon\cos(\phi) \end{Bmatrix} + \begin{Bmatrix} 0 \\ -\frac{1}{\varpi^2} \end{Bmatrix} \tag{8}$$

where $\tau = \omega t$, $\bar{x} = x/C$, $\bar{y} = y/C$, and $\varepsilon = e/C$.

Using Eqs. (3) and (8), the complete system of differential equations of motion may be written as follows:

$$\begin{aligned}
&\dot{\varepsilon} - \left[\pi\left(1-\varepsilon^2\right)^{2.5}\bar{f}_\varepsilon - 4\varepsilon\left(1-\varepsilon^2\right)^2\bar{f}_\phi\right]\frac{1}{\varpi\,\Gamma(\pi^2 + 2(\pi^2-8)\varepsilon^2)} = 0 \\
&\dot{\phi} + \frac{1}{2} - \left[4\left(1-\varepsilon^2\right)^2\bar{f}_\varepsilon - \frac{2\pi(1-\varepsilon^2)^{1.5}(1+2\varepsilon^2)}{\varepsilon}\bar{f}_\phi\right]\frac{1}{\varpi\,\Gamma(\pi^2 + 2(\pi^2-8)\varepsilon^2)} = 0 \\
&\ddot{\bar{x}} + \frac{\bar{K}}{\varpi^2}\left[1 - \frac{g(\tau)}{2}\left[\left(\Delta k_1 + \Delta k_2\cos(2\tau)\right)\left(\bar{x} - \varepsilon\sin(\phi)\right) + \Delta k_2\sin(2\tau)\left(\bar{y} + \varepsilon\cos(\phi)\right)\right]\right] = 0 \\
&\ddot{\bar{y}} + \frac{\bar{K}}{\varpi^2}\left[-\frac{g(\tau)}{2}\left(\Delta k_2\sin(2\tau)\right)\left(\bar{x} - \varepsilon\sin(\phi)\right) + \left(1 - \frac{g(\tau)}{2}\right)\left(\Delta k_1 - \Delta k_2\cos(2\tau)\right)\left(\bar{y} + \varepsilon\cos(\phi)\right)\right] + \frac{1}{\varpi^2} = 0
\end{aligned} \tag{9}$$

where $\bar{f}_\varepsilon$ and $\bar{f}_\phi$ are given by Eq. (2).

The system of equations (9) can be expressed as a system of six first-order differential equations of the following form:

$$\dot{X} = f(X; \Gamma, \varpi, \Delta k_\xi, \Delta k_\eta, \bar{K}) \tag{10}$$

where $X = (x_1, x_2, x_3, x_4, x_5, x_6)^{\mathrm{T}} = (\varepsilon, \phi, \bar{x}, \dot{\bar{x}}, \bar{y}, \dot{\bar{y}})^{\mathrm{T}}$. Therefore the system depends on five dimensionless parameters $(\Gamma, \varpi, \Delta k_\xi, \Delta k_\eta, \bar{K})$.

3. Numerical results and discussion

The dynamic response of the flexible cracked balanced rotor supported by hydrodynamic bearings is considered. The equations of motion (Eq. (9)) are integrated numerically using the Runge–Kutta method. To ensure that the data used to study the dynamic response of hydrodynamic bearings corresponds to a steady state, the data points for the first 800 revolutions of the rotor are not included in the figures. The dimensionless rotor speed ϖ is used as a control parameter in the bifurcation analysis. To investigate the effect of the crack, the balanced uncracked rotor is used as a reference. The dimensionless stiffness variation Δk_ξ and Δk_η of the shaft due to the crack are increased progressively. Three values of the dimensionless crack depth ratio defined in the nomenclature are considered, $r = 12\%$, $r = 25\%$, and $r = 50\%$, corresponding to three pairs of the dimensionless stiffness Δk_ξ and Δk_η, $(0.07, 0.02)$, $(0.2, 0.03)$ and $(0.4, 0.16)$ [14,15]. To determine the effect of the shaft crack on the dynamic response of the system, the dynamic trajectories of the journal center, bifurcation diagrams, Poincaré sections, and frequency spectra are plotted. The trajectory plot and the Poincaré sections are used to reveal the type of motion. The bifurcation diagram reveals the periodicity of the motion and the power spectrum is used to reveal the frequency content of the motion.

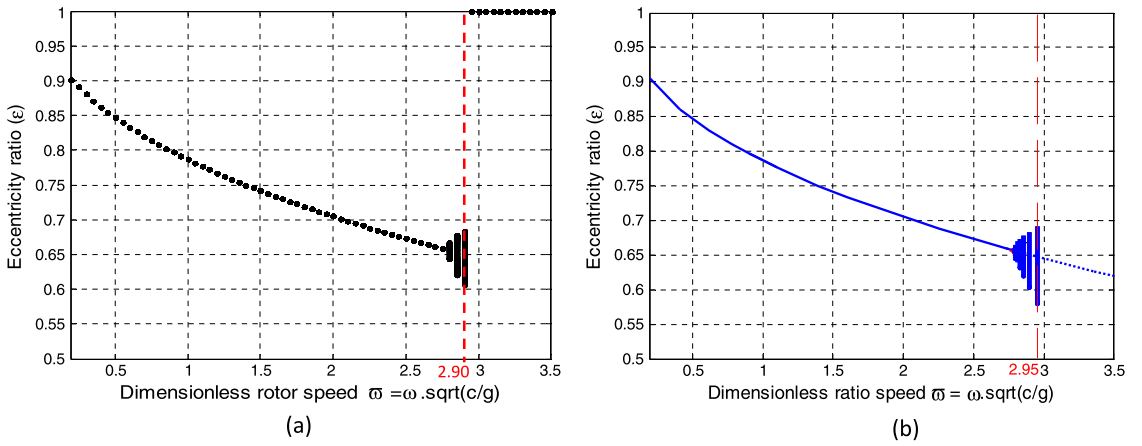

Fig. 3. Bifurcation diagrams of a balanced flexible rotor for $\Gamma = 0.1$ and $\bar{K} = 10$: (a) numerical integration, (b) numerical continuation.

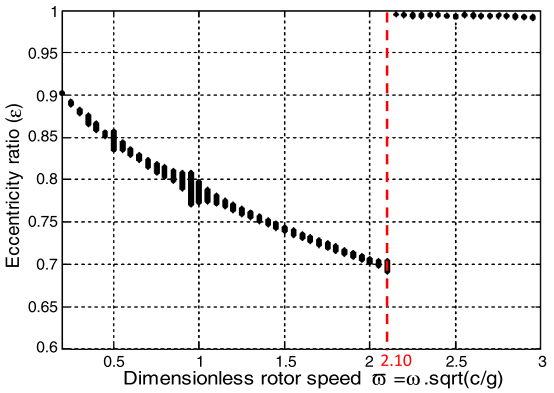

Fig. 4. Bifurcation diagram of the journal center of a balanced flexible cracked rotor for a small crack, $\Delta k_\xi = 0.07$, $\Delta k_\eta = 0.02$, $\Gamma = 0.1$ and $\bar{K} = 1$.

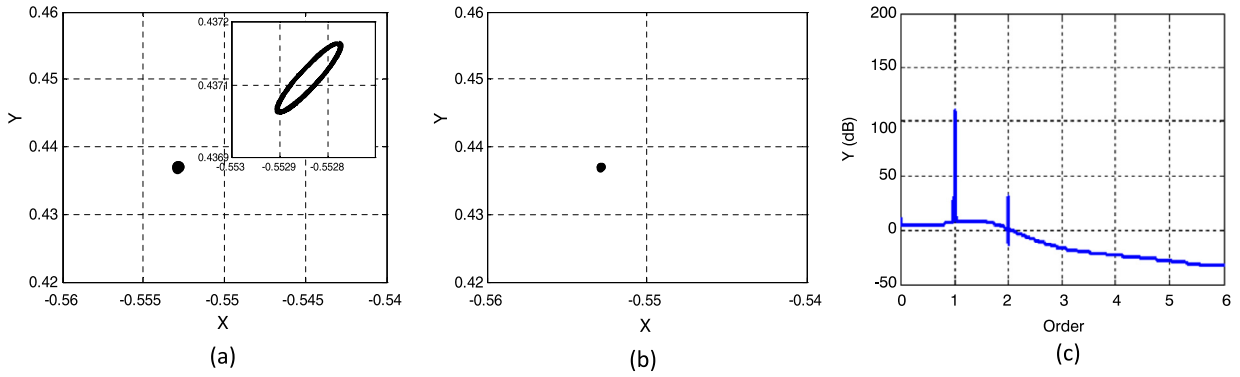

Fig. 5. Dynamic response of journal center of the uncracked rotor–bearing system for $\varpi = 2$, $\Gamma = 0.1$ and $\bar{K} = 1$: (a) trajectory of the journal center, (b) Poincaré section, (c) power spectrum.

To verify the validity of the results obtained by numerical integration, a comparative study is carried out with results obtained by numerical continuation using the Matlab toolbox MATCONT for the case of a flexible balanced rotor without a crack.

Figs. 2 and 3 show, respectively, the bifurcation diagram of the journal eccentricity for an increasing rotor speed ϖ for the bearing parameter $\Gamma = 0.1$ and for two shaft flexibilities $\bar{K} = 1$ and $\bar{K} = 10$. The figures show that the journal's steady-state stability limits obtained by numerical integration are in concordance with those obtained by numerical continuation.

Fig. 4 shows the bifurcation diagram obtained by numerical integration of a balanced cracked rotor for a small depth of the crack depicted by $r = 12\%$ for $\Gamma = 0.1$ and $\bar{K} = 1$. For $\varpi \leq 2.1$ the rotor is stable, but the journal's motion is different from that of the rotor without a crack, as shown in Fig. 2. For instance, the motion of the journal center of the

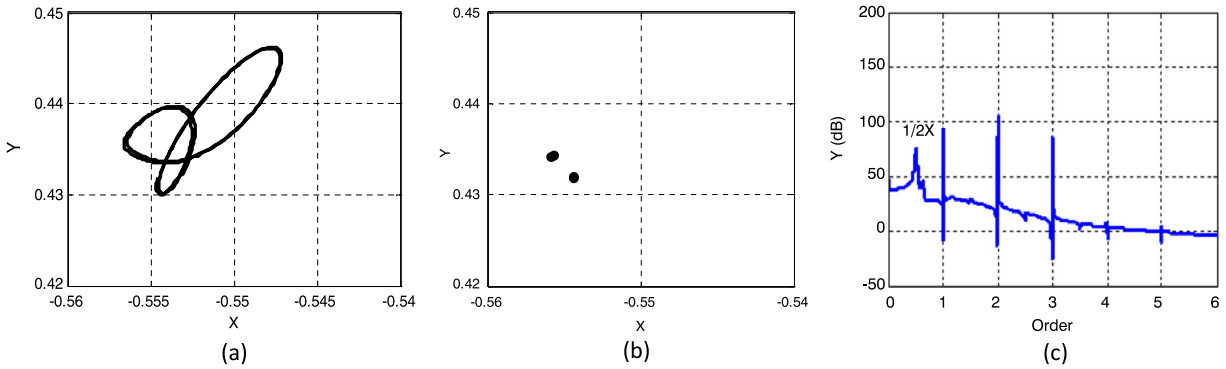

Fig. 6. Dynamic response of the journal center of the cracked rotor–bearing system for $\varpi = 2$, $\Gamma = 0.1$, $\Delta k_\xi = 0.07$, $\Delta k_\eta = 0.02$, and $\bar{K} = 1$: (a) trajectory of the journal center, (b) Poincaré section, (c) power spectrum.

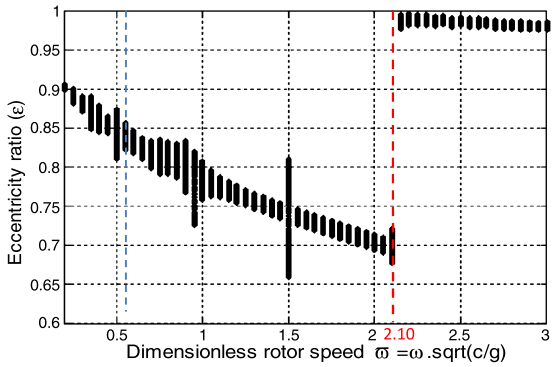

Fig. 7. Bifurcation diagram of a balanced flexible cracked rotor for a medium crack, $\Delta k_\xi = 0.2$, $\Delta k_\eta = 0.03$, $\Gamma = 0.1$, and $\bar{K} = 1$.

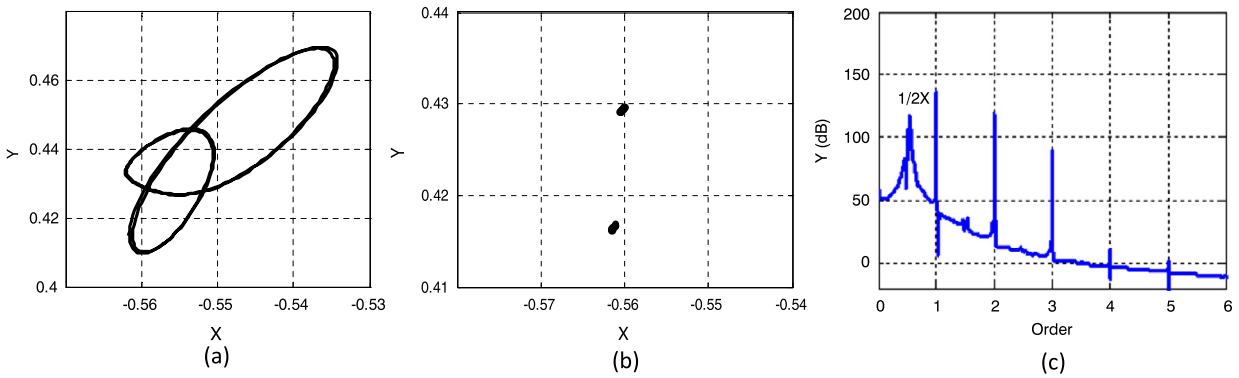

Fig. 8. Dynamic response of the cracked rotor–bearing system for $\varpi = 2$, $\Gamma = 0.1$, $\Delta k_\xi = 0.2$, $\Delta k_\eta = 0.03$, and $\bar{K} = 1$: (a) trajectory of the journal center, (b) Poincaré section, (c) power spectrum.

system without a crack is periodic for $\varpi = 2$, as shown in Fig. 5a–c. At the same value of ϖ, a double loop appears in the trajectory of the journal center, as shown in Fig. 6a, and the motion is $2T$ periodic (Fig. 6b), at half rotating frequency (Fig. 6c). The system loses its stability at $\varpi \approx 2.1$. For low values of the crack, the dynamic trajectory of the system changes, but the stability limit does not undergo a significant change. In this case, the use of the bifurcation diagram is not sufficient to prove the presence of a small crack. In order to show the influence of the crack, the trajectory of the journal center, the Poincaré section, and the power spectrum have to be used. The increase in the journal's amplitude of oscillation and the onset of a periodic double loop motion with a period corresponding to the half rotational speed are considered as indicators of the presence of a transverse crack.

Fig. 7 shows the bifurcation diagram for a medium crack depth for $r = 25\%$, $\Gamma = 0.1$, and $\bar{K} = 1$. The stability limit does not show any significant change compared to the system with a small crack depth (Fig. 4).

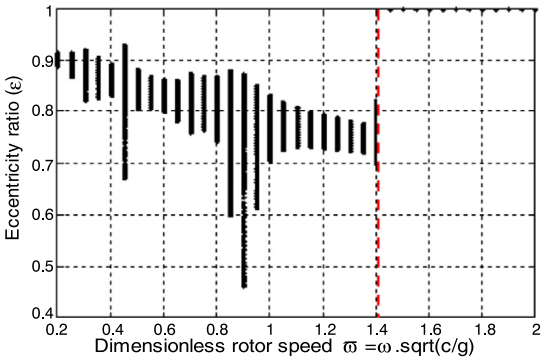

Fig. 9. Bifurcation diagram of a balanced flexible cracked rotor for a large crack, $\Delta k_\xi = 0.4$, $\Delta k_\eta = 0.16$, $\Gamma = 0.1$ and $\bar{K} = 1$.

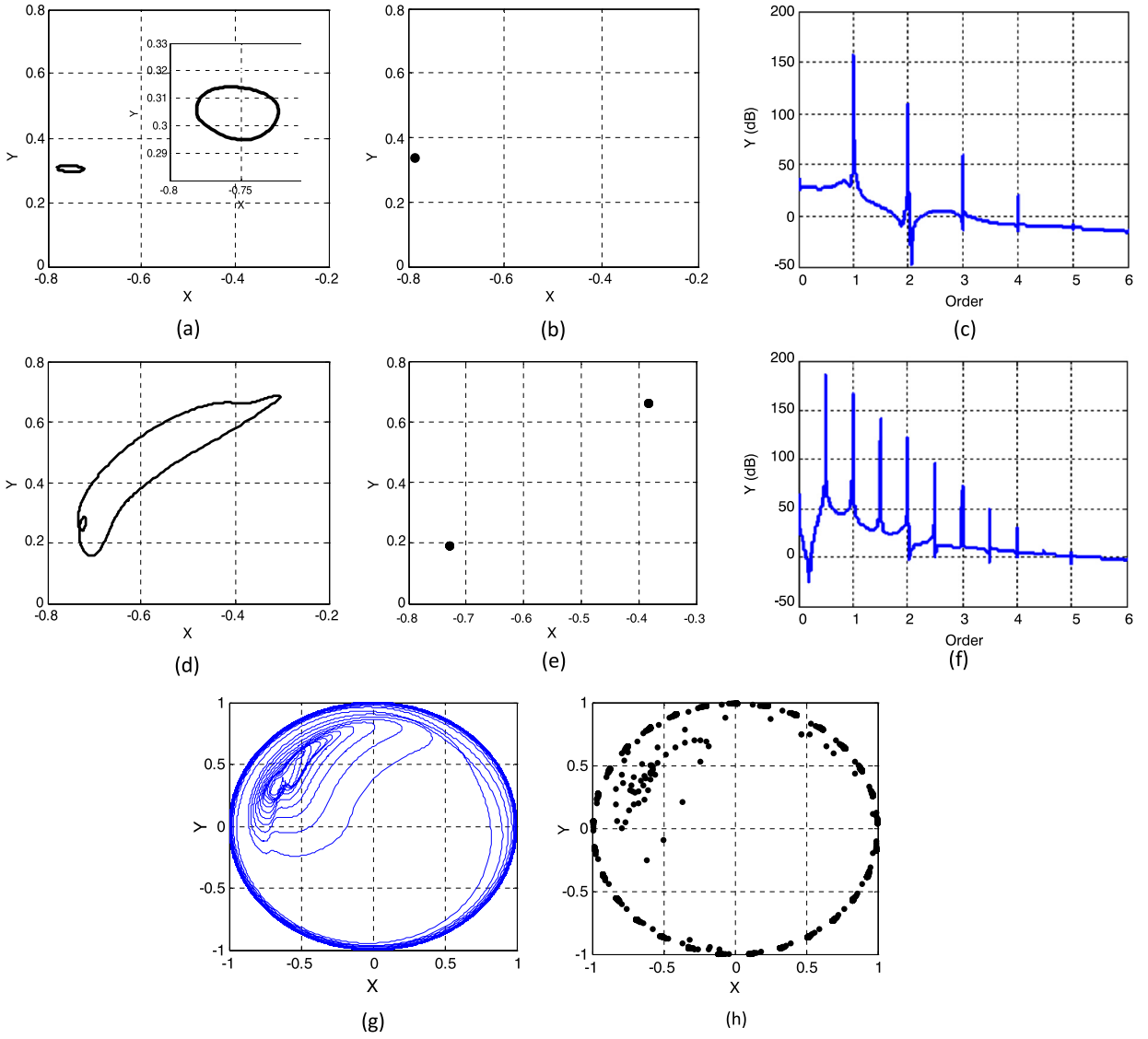

Fig. 10. Dynamic response of the cracked rotor–bearing system: trajectory of the journal center, Poincaré section, and power spectrum for $\varpi =$ 0.5, 1.4 and 1.45.

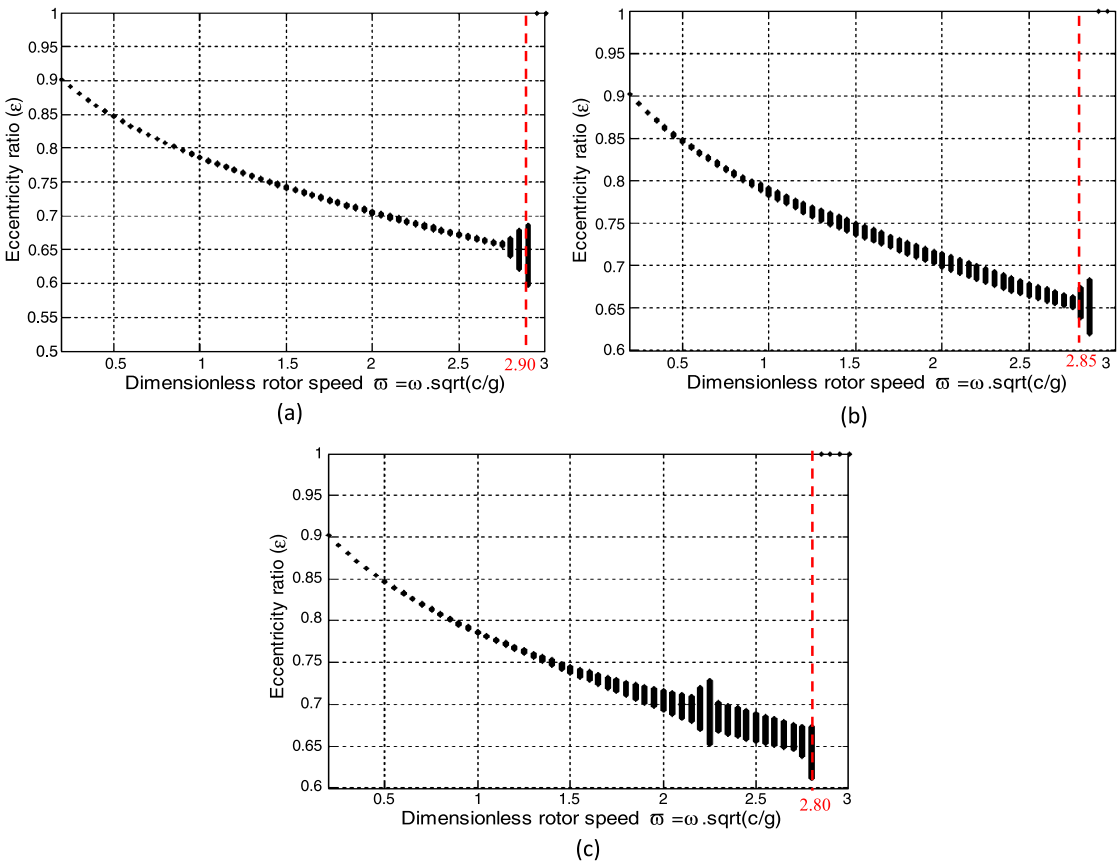

Fig. 11. Bifurcation diagram of a balanced flexible cracked rotor for $\Gamma = 0.1$ and $\bar{K} = 10$: (a) $\Delta k_\xi = 0.07$, $\Delta k_\eta = 0.02$, (b) $\Delta k_\xi = 0.2$, $\Delta k_\eta = 0.03$ and (c) $\Delta k_\xi = 0.4$, $\Delta k_\eta = 0.16$.

However, the increase in the depth of the crack affects the journal's motion. For example, for a rotor angular frequency $\varpi = 2$, the trajectory of the journal increases, two orbit appear (two points in the Poincaré section), and in the power spectrum, a new component has appeared on the one-half rotational frequency (Fig. 8 compared to Fig. 5).

For parameters corresponding to a larger rotor crack, $\Delta k_\eta = 0.4$ and $\Delta k_\xi = 0.16$, the stability critical speed ϖ decreases to 1.4 (Fig. 9). For $\varpi = 0.5$, the motion of the rotor is periodic (Fig. 10a–c). For $\varpi = 1.4$, the orbit is distorted and comprised of two loops of different sizes (Fig. 10d). The motion of the rotor also changes and becomes $2T$-periodic, as two points appear in the Poincaré section diagram, Fig. 10e. Spectral analysis shows that the amplitude of the one-half rotation frequency exceeds the amplitude of the rotation frequency (Fig. 10f). This proves the presence of a deeper crack on the shaft. The motion of the system becomes chaotic for $\varpi \geq 1.45$ (Fig. 10g–h).

Fig. 11 shows the bifurcation diagrams of the cracked rotor for a bearing parameter $\Gamma = 0.1$, shaft flexibility $\bar{K} = 10$ and three values of the dimensionless crack stiffness. The limit of stability of the system decreases with the increase in the depth of the crack (Fig. 11a–c).

For low crack depths ($r = 12\%$), the trajectory of the journal center is composed of two loops (Fig. 12a) for $\varpi = 2$. The motion of the rotor, depicted by the two points in the Poincaré section (Fig. 12b), is a $2T$-periodic. The presence of a component at one-half rotational frequency in the spectrum (Fig. 12c) proves the presence of the crack. In the vicinity of the stability limit, the center of the journal undergoes single loops with slight variations in their sizes (Fig. 12d). Several well points appear in the Poincaré section, which indicates that the motion is quasi-periodic (Fig. 12e). The structured amplitude of a one-third rotational frequency increases and exceeds the amplitude of the first rotational frequency (Fig. 12f). For $\varpi = 2.95$, the trajectory of the journal center diverges and the journal becomes in contact with the bearing (Fig. 12g); the motion becomes chaotic (Fig. 12h). These results agree qualitatively with the experimental results reported in the paper of Gómez-Mancilla [5] and Li Chaofeng [10], in which they have shown that the motion becomes quasi-periodic and the amplitudes of the one-third and one-half critical frequency increase and exceed the amplitude of the first rotational frequency. For a deeper crack ($r = 50\%$), A double periodic motion appears and the trajectory of the journal center becomes wider (Fig. 13a compared to Fig. 12a). The motion of the rotor is $2T$-periodic (Fig. 13b), and the amplitude of the rotational frequency increases (Fig. 13c compared to Fig. 12c). For $\varpi = 2.8$, the motion is quasi-periodic (Fig. 13d–e), and the ampli-

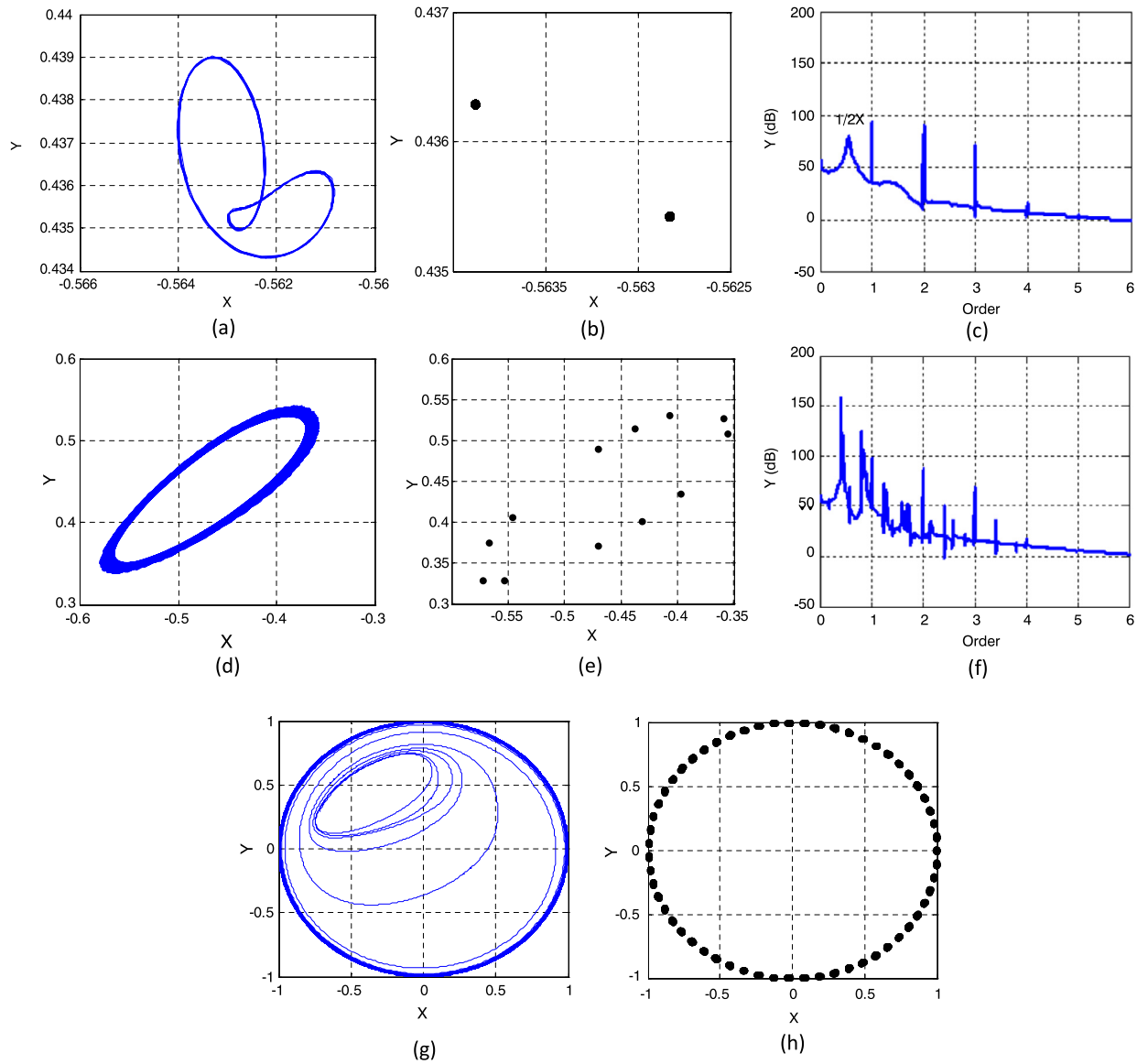

Fig. 12. Response of the cracked rotor–bearing system for $\Gamma = 0.1$, $\bar{K} = 10$, $\Delta k_\xi = 0.07$ and $\Delta k_\eta = 0.02$: trajectory of the journal center, Poincaré section and power spectrum for $\varpi = 2,\ 2.9,$ and 2.95.

Table 1
Stability limit of the journal center.

		Dimensionless depth ratio r			
	Γ	**0%**	**12%**	**25%**	**50%**
$\bar{K} = 1$	**1**	1.55	1.55	1.45	1.40
	0.1	2.10	2.10	2.10	1.40
	0.05	3.60	3.60	3.60	3.55
$\bar{K} = 10$	**1**	2.4	2.4	2.35	2.30
	0.1	2.9	2.9	2.85	2.80
	0.05	4.20	4.20	4.15	4.10

tude of the one-third rotational frequency exceeds the amplitude of the first rotational frequency (Fig. 13f). The motion of the system becomes chaotic for $\varpi = 2.85$ (Fig. 13g–h).

Table 1 presents the speed limits of stability ϖ for the three values of the bearing parameter Γ and the two values of the shaft flexibility. The limit of stability does not change significantly for low values of the crack depth. When the crack

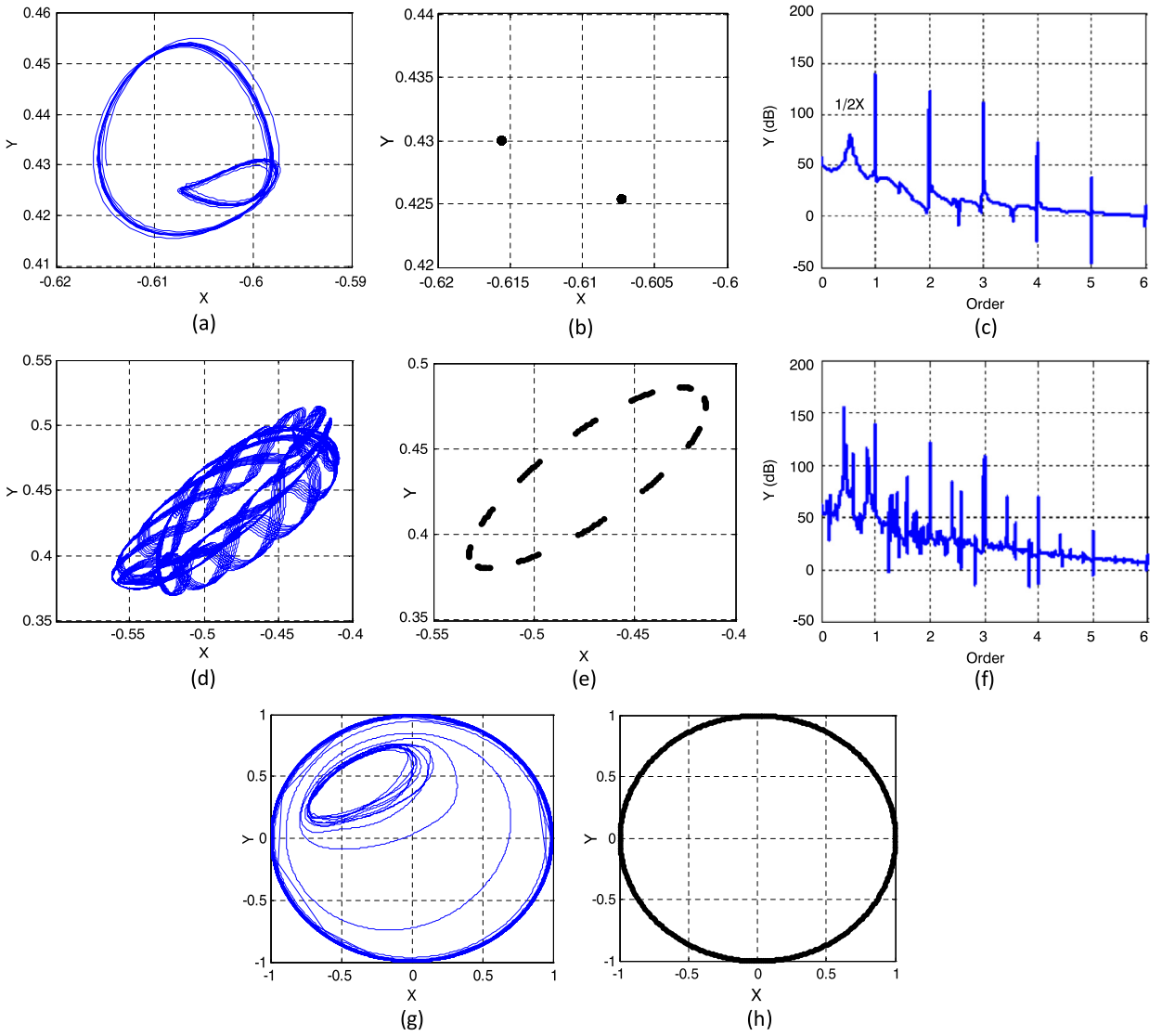

Fig. 13. Response of the cracked rotor–bearing system for $\Gamma = 0.1$, $\bar{K} = 10$, $\Delta k_\xi = 0.4$ and $\Delta k_\eta = 0.16$: trajectory of the journal center, Poincaré section and power spectrum for $\varpi = 2,\ 2.8$ and 2.85.

depth increases, the limit of stability decreases, especially for small values of Γ and low values of the flexibility $\bar{K}$. The presence of a crack has a limited effect on the stability limit for small values of the depth of the crack; however, it has an important effect on the dynamic response of the rotor. T-, $2T$-, $3T$-, …, nT-periodic motions of the rotor appear before the onset of instability.

4. Conclusion

A nonlinear dynamic analysis of balanced flexible cracked rotor–bearing systems is investigated. Bifurcation diagrams, Poincaré sections and trajectories of journal center are used to study the effect of the crack on the dynamic response and on the stability of the system. The presence of a crack in the shaft affects the orbit of the journal center and decreases the stability limit. A small crack has no significant effect on the stability limit, but affects the type of motion of the journal center. The appearance of one-third and one-half rotational frequency components in the spectrum and the increase of its amplitude at are considered an indicators of the presence of a crack in the rotor.

References

[1] A.S. Sekhar, Condition monitoring of cracked rotors through transient response, Mech. Mach. Theory 33 (1998) 1167–1175.
[2] C.A. Papadopoulos, A.D. Dimarogonas, Vibration of cracked shafts in bending, J. Sound Vib. 91 (1983) 583–593.

[3] A.S. Sekhar, B.S. Prabhu, Crack detection and vibration characteristics of cracked shafts, J. Sound Vib. 157 (1992) 375–381.
[4] W. Mayes, W.G.R. Davies, Analysis of the response of the multi-rotor–bearing system containing a transverse crack in a rotor, J. Vib. Acoust. 106 (1984) 139–145.
[5] J. Gómez-Mancilla, J.-J. Sinou, V.R. Nosov, F. Thouverez, A. Zambrano, The influence of crack-imbalance orientation and orbital evolution for an extended cracked Jeffcott rotor, C. R. Mecanique 332 (2004) 955–962.
[6] J.J. Sinou, A.W. Lees, The influence of cracks in rotating shafts, J. Sound Vib. 285 (2005) 1015–1037.
[7] J.J. Sinou, A.W. Lees, A non-linear study of a cracked rotor, Eur. J. Mech. A, Solids 26 (2007) 152–170.
[8] S. Xue, J. Cao, Nonlinear dynamic analysis of a cracked rotor–bearing system with fractional order damping, in: IDETC/CIE 2011, Washington DC, USA, 28–31 August, 2011.
[9] Y.G. Luo, S.H. Zhang, Dynamics analysis of nonlinear stiffness rotor–bearing system with crack fault, Res. J. Appl. Sci. Eng. Technol. 6 (11) (2013) 2093–2097.
[10] Chaofeng Li, Hexing Yu, Simulations and experimental investigation on motion stability of a flexible rotor–bearing system with a transverse crack, Chin. J. Mech. Eng. 26 (6) (2013) 1194–1203.
[11] Robert Gasch, Dynamic behaviour of the Laval rotor with a transverse crack, Mech. Syst. Signal Process. 22 (2008) 790–804.
[12] J. Wang, On the stability of rotor–bearing systems based on Hopf bifurcation theory, PhD thesis, Louisiana State University, Baton Rouge, LA, USA, 2005.
[13] J. Frêne, D. Nicolas, B. Degueurce, D. Berthe, M. Godet, Hydrodynamic Lubrication Bearings and Thrust Bearings, Tribology Series, Elsevier, Amsterdam, 1997.
[14] J.C. Gomez-Mancilla, J.M. Machorro-Lopez, Local resonance of crack-imbalance orientations and orbital evolution to detect mid-span rotor cracks: part 2 experimental validations, in: Proc. IMAC-XXIII, Orlando, FL, USA, 2005.
[15] R. García-Illescas, J. Gómez-Mancilla, V. Nosov, Vibration analysis in the characterization of the dynamic behaviour of cracked rotating shafts, in: Proc. Int. Conf. on Rotating Machinery, IFToMM, Sydney, Australia, 2002.